Persistence of Tertiary Structure in 7.9 M Guanidinium Chloride: The Case of Endo-β-1,3-glucanase from *Pyrococcus furiosus*[†]

Roberta Chiaraluce,[‡] John van der Oost,[§] Joyce H. G. Lebbink,[||] Thijs Kaper,[§] and Valerio Consalvi*,[‡]

Dipartimento di Scienze Biochimiche A Rossi Fanelli, Università la Sapienza, Piazzale Aldo Moro 5, 00185 Rome, Italy, Laboratory of Microbiology, Wageningen University, H. van Suchtelenweg 4, 6703 CT Wageningen, The Netherlands, and Department of Molecular Carcinogenesis, Netherlands Cancer Institute, Plesmanlaan 121, 1066 CX Amsterdam, The Netherlands

Received July 23, 2002; Revised Manuscript Received October 7, 2002

ABSTRACT: The *Pyrococcus furiosus* endo-β-1,3-glucanase belongs to the subfamily of laminarinase, which can be classified as "all β proteins" as confirmed by deconvolution of far-UV CD and FTIR spectra. The persistence of a significant amount of tertiary structure in 7.9 M GdmCl, as indicated by near-UV CD spectroscopy, accompanied by a red-shift of the maximum fluorescence emission wavelength is a peculiar property of this hyperthermophilic endoglucanase. The possibility to observe tertiary structure elements under extremely denaturing conditions is notable and is limited to only a few examples. The unusual resistance toward guanidinium chloride denaturation is paralleled by a notable stability at extremely low pH and at high temperature. The analysis of the protein spectral properties indicates that the secondary structure elements are preserved down to pH 1.0 and up to 90 °C at pH 7.4 and pH 3.0. The study of the conditions that determine the persistence of residual structure at high denaturant concentration and the examination of these structures are particularly interesting because these state(s) may be preliminary or coincident with the coalescence of protein aggregates or to the formation of amyloid-like fibrils, and they may serve as seeds of protein folding.

The most thermostable endo-β-1,3-glucanase (endoglucanase)[1] described so far is the secreted endoglucanase from the hyperthermophilic archaeon *Pyrococcus furiosus* (*1*). The extreme thermal resistance (half-life at 100 °C is 16 h) and the temperature optimum for catalysis at 100−105 °C make this enzyme an attractive target for stability studies and to monitor the effect of temperature on its structure in solution. Thermal stability studies may lead to a better comprehension of the structural determinants required for this outstanding molecular adaptation at high temperature. In turn, the analysis of the structural changes induced by temperature may offer clues to understand the thermal resistance or to recognize the transitions that are preliminary to irreversible inactivation.

The *P. furiosus* endoglucanase belongs to the subfamily of laminarinase in the glycosyl hydrolase family 16, according to a sequence-based classification (*2*). This type of classification reflects the structural features of the enzymes since the members of a family share a similar three-dimensional structure and a similar fold, despite important differences in the region surrounding the conserved catalytic residues (*2*, *3*). These bacterial glucanases belong to the class of "all β proteins" (*4*) and fold like the concanavalin A-like lectins into a compact jellyroll-type β-sheet structure. Several of these enzymes, independent of the thermophilic origin, are remarkably stable against thermal inactivation (*3*, *5*). Moreover, a particular interest for this class of protein arises from its potential biotechnological value (*6*, *7*). The main interest derives from the fact that the enzyme is able to hydrolyze complex glucose polymers into smaller oligomers. Its capability to resist against thermal and acid denaturation is advantageous in some industrial applications (*3*).

These premises led us to study the stability in solution of the endoglucanase from *P. furiosus* at different pH values and at increasing temperatures and guanidinium chloride (GdmCl) concentration by the use of several spectroscopic techniques to follow the protein structural transitions induced by solvent and temperature changes. In the course of studying the denaturation process, some interesting properties of this enzyme were observed. In the presence of 7.9 M GdmCl, the spectral features indicative of the enzyme's tertiary structure are not completely abolished, and at extremely low pH a significant amount of tertiary structure is also present. The possibility to observe the tertiary structure under extremely denaturing conditions is notable and is limited to only a few examples (*8*, *9*). The study of the conditions that determine the persistence of residual structure at high denaturant concentration and the examination of these structures are particularly interesting because these state(s)

[†] This research was supported by the Italian Ministero Istruzione Università Ricerca (MIUR) and Contract BIO 4-CT96-0488 of the European Union.

* Corresponding author e-mail: consalvi@caspur.it; phone: +39 064 9910939; fax: +39 064 440062.

[‡] Università la Sapienza.

[§] Wageningen University.

[||] Netherlands Cancer Institute.

[1] Abbreviations: ANS, 8-anilinonaphthalene-1-sulfonic acid; endoglucanase, endo-β-1,3-glucanase; GdmCl, guanidinium chloride.

10.1021/bi026498u CCC: $22.00
Published on Web 11/14/2002

may be preliminary or coincident with the coalescence of protein aggregates or to the formation of amyloid-like fibrils (*10*, *11*), and in turn, they may serve as seeds of protein folding (*8*, *9*).

MATERIAL AND METHODS

Chemicals and Buffers. GdmCl, 8-anilinonaphthalene-1-sulfonic acid ammonium salt (ANS), DTT, EDTA, and laminarin were from Fluka. 3′,5′-Dinitrosalicylic acid was purchased from Sigma. Buffer solutions were filtered (0.22 μm) and carefully degassed. All buffers and solutions were prepared with ultra-high-quality water (ELGA UHQ, U.K.).

Enzyme Preparation and Assay. The *P. furiosus* endoglucanase was functionally produced in *Escherichia coli* BL21-(DE3) with pLUW530, as described before (*1*). Purification of the enzyme was performed according to ref *1* with an additional size-exclusion chromatography step on Superdex 75 (Amersham Pharmacia). The protein concentration was determined at 280 nm using $\epsilon_{280} = 82030\ M^{-1}\ cm^{-1}$ calculated according to Gill and von Hippel (*12*). Endoglucanase activity was determined by measuring the amount of reducing sugars released upon enzyme incubation in the presence of laminarin as described by Guegen et al. (*1*). The enzyme was incubated in 0.1 M sodium phosphate buffer, pH 6.5, containing 0.5% (w/v) laminarin at 80 °C for 10 min. One unit of enzyme activity is defined as the amount of endoglucanase catalyzing the formation of 1 μmol of reducing sugars/min under the above-defined conditions; glucose was used as a standard.

Spectroscopic Techniques. Intrinsic fluorescence emission and light-scattering measurements were carried out with a LS50B Perkin-Elmer spectrofluorimeter using a 1-cm path length quartz cuvette. Fluorescence emission spectra were recorded at 300−450 nm (1-nm sampling interval) at 20 °C with the excitation wavelength set at 290 nm. Light scattering was measured at 20 °C with both excitation and emission wavelengths set at 480 nm.

Far-UV (180−250 nm) and near-UV (250−310 nm) CD measurements were performed in 0.01−0.2- and 1.0-cm path length quartz cuvettes, respectively. CD spectra were recorded on a Jasco J-720 spectropolarimeter. The results are expressed as the mean residue ellipticity ([Θ]) assuming a mean residue weight of 110 per amino acid residue. In all the spectroscopic measurements at pH 7.4, 100 μM EDTA was present unless otherwise stated.

FTIR spectra were recorded on a Nicolet Magna 760 spectrometer (Nicolet) equipped with a MCT detector. Solution ATR spectra were measured in a CIRCLE cell (Spectra Tech, Madison, WI) thermostated at 20 °C. Protein samples (120 μL) of a 8 mg/mL protein solution in 20 mM Tris-HCl at pH 7.4 or pH 2.0 (10 mM HCl) were placed in the CIRCLE cell with a Si crystal rod. A total of 512 interferograms at 2 cm^{-1} resolution were collected for each spectrum, with Mertz apodization and two levels of zero filling. The sample chamber of the spectrometer was continuously purged with dry air to avoid water vapor interference on the bands of interest. The background spectra were collected immediately before the sample measurements and under the same conditions with the cell filled with everything but protein. At the end of the measurements, after prolonged washing, a spectrum of the cell was recorded to check for protein absorption on the Si crystal rod (*13*). Water vapor spectra were collected by reduction of the dry-air purge of the clean cell.

Experiments with the fluorescent dye ANS were performed at 20 °C by incubating the protein and ANS at 1:5 molar ratio. After 5 min, fluorescence emission spectra were recorded at 400−600 nm with the excitation wavelength set at 390 nm. The maximum fluorescence emission wavelength and the intensity of the hydrophobic probe ANS depend on the environmental polarity (e.g., on the hydrophobicity of the accessible surface of the protein) (*14*).

GdmCl-Induced Unfolding and Refolding. For equilibrium transition studies, the enzyme (final concentration 40−60 μg/mL) was incubated at 20 °C at increasing concentrations of GdmCl (0−8 M) in 20 mM Tris-HCl, pH 7.4, in the presence of 100 μM DTT and 100 μM EDTA or in 10 mM HCl (pH 2.0). After 24 h, equilibrium was reached and intrinsic fluorescence emission and far-UV CD spectra (0.2-cm cuvette) were recorded in parallel at 20 °C. To test the reversibility of the unfolding, endoglucanase was unfolded at 20 °C in 7.8 M GdmCl at 0.8 mg/mL protein concentration in 25 mM Tris-HCl, pH 7.4, in the presence of 100 μM DTT and 100 μM EDTA or in 10 mM HCl (pH 2.0). After 24 h, refolding was started by 20-fold dilution of the unfolding mixture at 20 °C into solutions of the same buffer used for unfolding containing decreasing GdmCl concentrations. The final enzyme concentration was 40 μg/mL. After 24 h, intrinsic fluorescence emission and far-UV CD spectra were recorded at 20 °C.

Acid-Induced Denaturation. *P. furiosus* endoglucanase was incubated 2 h in HCl at pH 3.0, 2.0, and 1.0. The pH of the solution was measured with an InLab 422 electrode (Mettler-Toledo AG) connected to a Corning P 507 ion meter before and after the addition of the enzyme; pH adjustments were not required.

Thermal Denaturation. For thermal scans, the protein samples (0.2 mg/mL) at pH 7.4, 3.0, and 2.0 were heated from 10 to 95 °C and subsequently cooled to 10 °C with a heating/cooling rate ranging from 0.75 to 1.50 deg/min controlled by a Jasco programmable Peltier element in a 0.1-cm cuvette. A scan rate of 1 deg/min was chosen in consideration of the observed independence of thermal transitions on the heating/cooling rate. Far-UV CD spectra were recorded every 5−2.5 °C, and the dichroic activity at 222 nm was continuously monitored every 0.5 °C with 4-s averaging time. All the spectra were corrected for solvent contribution at increasing temperature for all the different pH values examined. The presence of aggregated particles at the end of the thermal transitions was controlled by 90° light-scattering and size-exclusion chromatography.

The thermal transition at pH 2.0 were monitored by FTIR spectroscopy in the same CIRCLE cell used at 20 °C. A carefully degassed protein sample (8 mg/mL) was loaded by a Teflon tubing loop that was sealed before monitoring the thermal transition. The cell was heated from 10 to 90 °C and cooled to 20 °C with a 10-deg interval at a heating rate of 1 °C/min by a programmable Julabo FP50-HP circulation water bath. The spectra were corrected for solvent and water vapor contribution at each temperature interval.

Data Analysis. The changes in intrinsic fluorescence emission spectra at increasing GdmCl concentrations were

quantified as the intensity-averaged emission wavelength, $\bar{\lambda}$, (*15*) calculated according to

$$\bar{\lambda} = \sum(I_i\lambda_i)/\sum(I_i) \quad (1)$$

where λ_i and I_i are the emission wavelength and its corresponding fluorescence intensity at that wavelength, respectively.

Far-UV CD spectra from GdmCl titration were analyzed by the singular value decomposition algorithm (SVD) (*16*−*18*) using the software MATLAB (MathWorks, South Natick, MA). SVD is useful to find the number of independent components in a set of spectra and to remove the high-frequency noise and the low-frequency random error. CD spectra in the 210−250-nm region (0.2-nm sampling interval) were placed in a rectangular matrix **A** of *n* columns, one column for each spectrum collected in the titration. The **A** matrix is decomposed by SVD into the product of three matrices: $\mathbf{A} = \mathbf{U} \times \mathbf{S} \times \mathbf{V}^T$ where **U** and **V** are orthogonal matrices and **S** is a diagonal matrix. The columns of **U** matrix contain the basis spectra, and the columns of the **V** matrix contain the denaturant dependence of each basis spectrum. Both **U** and **V** columns are arranged in terms of their decreasing order of the relative weight of information, as indicated by the magnitude of the singular values in **S**. The diagonal **S** matrix contains the singular values that quantify the relative importance of each vector in **U** and **V**. An important feature of SVD analysis is that the signal-to-noise ratio is very high in the earliest columns of **U** and **V** and that the random noise is mainly accumulated in the latest **U** and **V** columns. The wavelength-averaged spectral changes induced by increasing denaturant concentrations are represented by the columns of matrix **V**. Therefore, the plot of the columns of **V** versus the denaturant concentration provides information about the observed transition.

The FTIR spectra were analyzed using GRAMS software (Galactic Industries Corp., Salem, NH). The water vapor contribution was subtracted from each of the sample spectra. The essentially featureless region between 1700 and 1800 cm^{-1} (where no protein bands are present) indicated that water vapor components are not responsible for the observed bands in the amide I region. The individual components in the amide region were identified by second derivative and Fourier self-deconvolution of the raw spectrum using GRAMS. Curve-fitting of the raw spectrum with a mixed Gaussian−Lorentzian function was then performed to determine the peak positions and parameters of each individual component. The assignments of the component bands to secondary structure elements were based on the literature (*19*−*28*), and the area under each peak was used to calculate the percentage of secondary structure components.

GdmCl-induced equilibrium unfolding was analyzed by fitting baseline and transition region data to a two-state linear extrapolation model (*29*) according to

$$\Delta G_{unfolding} = \Delta G^{H_2O} + m_g[\text{GdmCl}] = -RT \ln K_{unfolding} \quad (2)$$

where $\Delta G_{unfolding}$ is the free energy change for unfolding for a given denaturant concentration, ΔG^{H_2O} is the free energy change for unfolding in the absence of denaturant, m_g is a slope term that quantitates the change in $\Delta G_{unfolding}$ per unit concentration of denaturant, *R* is the gas constant, *T* is the temperature, and $K_{unfolding}$ is the equilibrium constant for unfolding. The model expresses the signal as a function of denaturant concentration:

$$y_i = \frac{y_N + m_N[X]_i + (y_D + m_D[X]_i)\exp[(-\Delta G^{H_2O} - m_g[X]_i)/RT]}{1 + \exp[(-\Delta G^{H_2O} - m_g[X]_i)/RT]} \quad (3)$$

where y_i is the observed signal, y_N and y_D are the native and denatured baseline intercepts, m_N and m_D are the native and denatured baseline slopes, $[X]_i$ is the denaturant concentration after the *i*th addition, ΔG^{H_2O} is the extrapolated free energy of unfolding in the absence of denaturant, m_g is the slope of a ΔG unfolding versus [X] plot, *R* is the gas constant, and *T* is the temperature. $[\text{GdmCl}]_{0.5}$ is the denaturant concentration at the midpoint of the transition and, according to eq 2, is calculated as follows:

$$[\text{GdmCl}]_{0.5} = \Delta G^{H_2O}/m_g \quad (4)$$

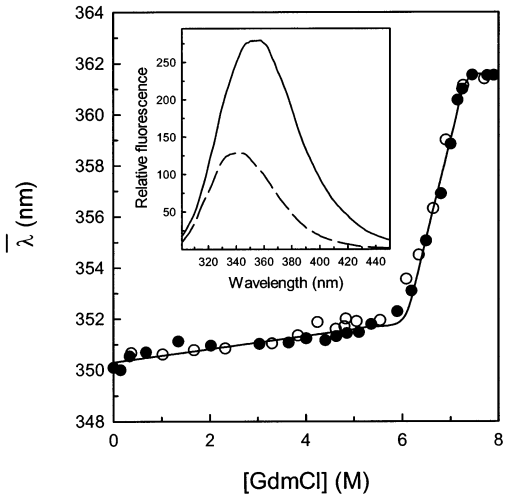

FIGURE 1: GdmCl-induced fluorescence changes of *P. furiosus* endoglucanase. Fluorescence changes are reported as $\bar{\lambda}$, calculated according to eq 1. Continuous line is the nonlinear regression to eq 3 of the fluorescence data at varying denaturant concentration as described in the text (see Materials and Methods). The reversibility points (empty symbols) were not included in the nonlinear regression analysis. The inset shows the spectra of the native (dashed line) and of the enzyme in 8 M GdmCl (solid line). All the spectra were recorded at 20 °C after 24-h incubation.

RESULTS

Equilibrium Transition Studies in GdmCl at pH 7.4. Incubation of endoglucanase at increasing GdmCl concentrations (0−8 M) in 25 mM Tris-HCl, pH 7.4, containing 200 μM DTT and 100 μM EDTA for 20 h at 20 °C resulted in a progressive increase in intrinsic fluorescence emission intensity. In the native state, endoglucanase exhibits a fluorescence emission maximum at 342 nm when excited at 290 nm. At the end of the transition, the intrinsic fluorescence emission intensity was increased 2-fold as compared to that of the native enzyme, and the maximum fluorescence emission wavelength was shifted to 357 nm (Figure 1). The red-shift of the intrinsic fluorescence emission was determined by calculation of the intensity-averaged emission wavelength ($\bar{\lambda}$) according to eq 1. This quantity is an integral measurement, negligibly influenced by the noise, which reflects changes in the shape and position of the emission

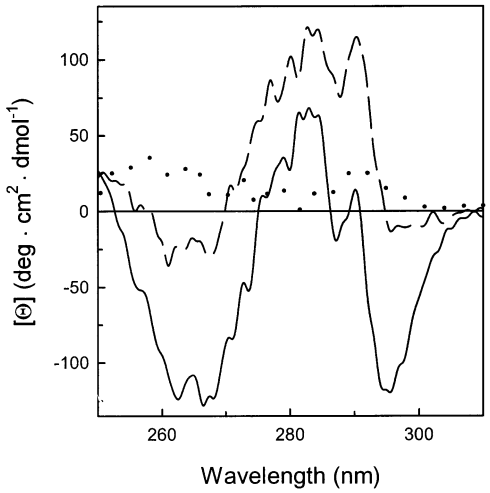

FIGURE 2: Effect of GdmCl on the near-UV CD spectrum of *P. furiosus* endoglucanase. Near-UV CD spectra were recorded at 20 °C in a 1-cm quartz cuvette at 0.6 mg/mL protein concentration after 24-h incubation of the protein in 20 mM Tris-HCl at pH 7.4 (—), 7.9 M GdmCl at pH 7.4 (− −), and 7.9 M GdmCl at pH 2.0 (•••).

spectrum. A plot of $\bar{\lambda}$ as a function of the GdmCl concentration showed a sigmoidal denaturant dependence with a transition midpoint at 6.7 ± 0.05 M (Figure 1). The sigmoidal denaturation curve shown in Figure 1 indicates that the process follows a two-state mechanism without any detectable intermediates. The fluorescence changes were reversible, as indicated by the identity of the variations in the intensity-averaged emission wavelength ($\bar{\lambda}$) monitored during the transitions (Figure 1). The enzyme activity was fully recovered after dilution of the denaturant. The ΔG^{H_2O} and m_g values were 15.4 and 2.3 kcal mol^{-1} M^{-1}, respectively, as calculated by nonlinear regression fitting of the data reported in Figure 1 according to eqs 3 and 4. The ΔG^{H_2O} value is at the upper limit for a folded globular protein (i.e., 5−15 kcal/mol (*30*)), indicating the extreme stability of the *P. furiosus* enzyme.

Far-UV CD spectra were unchanged upon the increase of GdmCl concentration (data not shown). This result was confirmed by the reconstitution of the spectra after SVD data analysis and by the random variation in magnitude and sign of the two most significant columns of the **V** matrix as a function of denaturant concentration. The lack of any measurable change by far-UV CD spectroscopy after incubation of the enzyme in 7.9 M GdmCl, despite the large modification of its intrinsic fluorescence properties, led to study the tertiary structure arrangement by near-UV CD. The near-UV CD spectrum of endoglucanase monitored after incubation at pH 7.4 in 7.9 M GdmCl (Figure 2) shows that the 295-nm negative band is almost completely suppressed, the amplitude of the negative ellipticity signal in the 260−270-nm region is significantly reduced, and the fine-structure features of the 275−290-nm region are preserved with an increase in positive ellipticity. These results indicate that in 7.9 M GdmCl at pH 7.4 the tertiary structure arrangement is altered but not completely suppressed. Incubation of *P. furiosus* endoglucanase at increasing urea concentrations (0−9.9 M) did not result in any change of the enzyme spectral properties. A complete suppression of the tertiary structure requires the incubation of endoglucanase in 7.9 M GdmCl at pH 2.0 (10 mM HCl) (Figure 2).

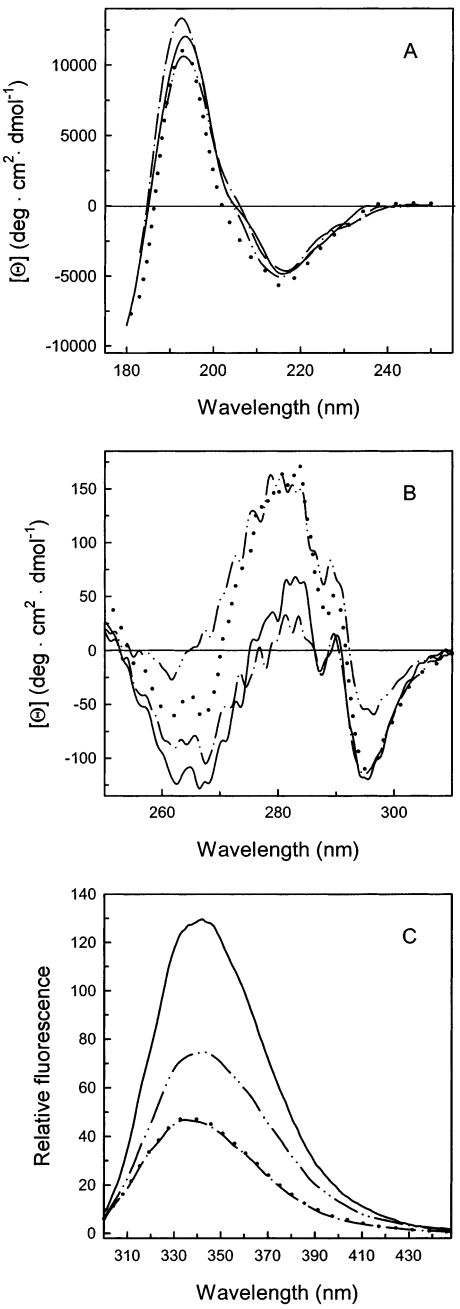

FIGURE 3: Effect of pH on the spectral properties of *P. furiosus* endoglucanase. (A) Far-UV CD spectra were recorded in a 0.01-cm quartz cuvette at 1.0 mg/mL. (B) Near-UV CD spectra were recorded in a 1-cm quartz cuvette at 0.6 mg/mL protein concentration. (C) Fluorescence spectra were recorded at 40 μg/mL protein concentration (290 nm excitation wavelength). All the spectra were recorded at 20 °C after 24-h incubation of the protein at pH 7.4 (20 mM Tris-HCl, —), pH 3.0 (1.0 mM HCl, •••), pH 2.0 (10.0 mM HCl, − • −), and pH 1.0 (100.0 mM HCl, − •• −).

Effect of pH on the Enzyme Structure. The far-UV CD spectrum of the *P. furiosus* endoglucanase at pH 7.4 shows a local minimum at 215 nm and a maximum near 194 nm, typical for a protein with a significant content of β structure (*31*, *32*). The spectrum is generally unchanged after 2-h incubation, a time that was established to be sufficient to reach equilibrium, at pH 3.0, 2.0 and 1.0 at 20 °C (Figure 3A) whereas the near-UV CD (Figure 3B) and the intrinsic fluorescence emission (Figure 3C) spectra show different profiles depending on the pH. At pH 3.0, the positive 272−

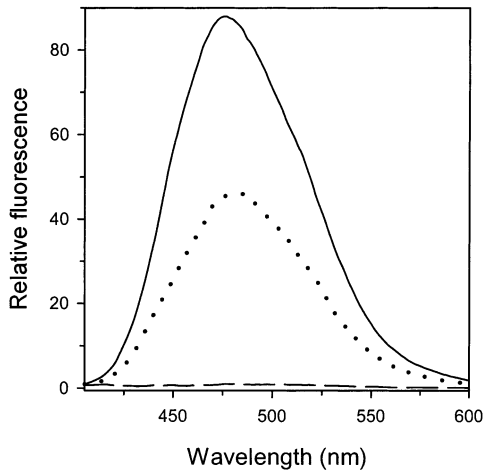

FIGURE 4: Relative accessibility of hydrophobic residues in *P. furiosus* endoglucanase monitored by the extrinsic fluorescence of ANS. ANS (7.5 μM) was added to the protein (1.5 μM) previously incubated 24 h at pH 7.4 (20 mM Tris-HCl, dashed line), pH 3.0 (1.0 mM HCl, dotted line), and pH 2.0 (10.0 mM HCl, continuous line). Fluorescence emission spectra (390 nm excitation wavelength) were recorded at 20 °C 10 min after the addition of ANS.

284-nm region is modified in comparison with the enzyme at neutral pH. The same alteration is observed in the near-UV CD spectrum of the protein at pH 1.0, which in addition shows a significant reduction in the amplitude of the negative dichroic bands at 266−272 and 295 nm (Figure 3B). At pH 2.0, the near-UV CD spectrum is comparable to that of the enzyme at pH 7.4 with a minor change centered around 284 nm. The intrinsic fluorescence emission spectra of endoglucanase at pH 2.0 and pH 3.0 are closely similar, and both reveal a 2.8-fold decrease of the fluorescence intensity accompanied by a blue-shift of the maximal emission wavelength from 342 to 335 nm in comparison with the enzyme at pH 7.4 (Figure 3C). At pH 1.0, the maximal emission wavelength is the same as that at pH 7.4, but the fluorescence intensity is 1.7-fold decreased (Figure 3C). The changes in the intrinsic fluorescence emission spectra induced by acidic pH confirm that the tertiary structure is perturbed locally but not completely suppressed.

The accessibility of hydrophobic residues upon incubation of *P. furiosus* endoglucanase at pH 2.0 and pH 3.0 was analyzed by the fluorescent probe anilinonaphthalene-8-sulfonic acid (ANS). The fluorescence emission spectrum of ANS shows a notable increase in intensity and a blue-shift from 510 to 477 and 483 nm in the presence of the protein at pH 2.0 and pH 3.0, respectively (Figure 4), suggesting that at pH 2.0, despite the presence of a nativelike near-UV CD signal, the protein shows an increased exposure of hydrophobic surface area.

Estimation of the Enzyme Secondary Structure. The relative content of the secondary structure elements in solution, estimated by SELCON 2 (*33*) on the far-UV CD spectra at pH 7.4, 3.0, 2.0, and 1.0 was at least 96% and ranged over 5.8−8.4% α, 43.6−46.9% β, 20−26% turns, 3.1−5% polyproline II, and 15.9−22.4% of other structures (Table 1). The relative amount of α and β structure was also consistent with that determined by K2D program (*34*). These results indicate that the endoglucanase relative secondary structure composition is not significantly affected by a pH decrease up to 1.0.

Table 1: Relative Content of *P. furiosus* Endoglucanase Secondary Structure Estimated by SELCON 2

pH	α (%)	β (%)	turns (%)	PolyProII (%)	other (%)	total (%)
7.4	6.3	45.0	19.0	5.0	22.4	97.7
3.0	8.4	45.0	25.0	5.5	15.9	99.8
2.0	5.8	46.9	21.3	5.1	20.9	100
1.0	8.3	43.6	23.4	3.1	17.6	96.0

The relative secondary structure content was also analyzed by FTIR spectroscopy after deconvolution of the amide I region. At pH 7.4 seven individual peaks were observed, centered at 1689, 1680, 1670, 1664, 1653, 1632, and 1614 cm^{-1} (Figure 5A). The main peak at 1632 cm^{-1} can be assigned to β-sheets (*23*, *24*) and corresponded to 53.0% of the total area of the amide I region (Table 2). The higher estimation of relative β-sheets content as compared to that obtained by SELCON 2 on far-UV CD spectra (Table 1) may be attributed to the fact that in FTIR spectra the PolyProII band can overlap with the 1632 cm^{-1} band (*35*). The peak at 1653 cm^{-1}, 28.0% of the amide I, is in a spectral region where α-helices and unordered structure can equally contribute (*21*, *23*, *24*). The peak at 1689 was assigned to antiparallel β-sheets and aggregated strands and corresponded to 2.1% of the total area of the amide I region (*24*, *26*, *28*). The peaks at 1680, 1670, and 1664 cm^{-1} were assigned to turns (*22*−*25*, *28*) and corresponded to 16.9% of the total area of the amide I region. The peak at 1614 cm^{-1} can be assigned to the vibrations of the tyrosine ring (*36*). At pH 2.0 the amide I region is closely similar to that at pH 7.4, and the deconvolution of the region showed only minor structural changes localized in the 1690−1660-cm^{-1} region (Table 2) and a modest increase at 1614 cm^{-1}(Figure 5B). The similarity in secondary structure elements at pH 7.4 and pH 2.0 is on line with the results obtained by far-UV CD spectroscopy. Secondary structure prediction, performed according to Rost (*37*), shows the presence of two α-helices in the regions corresponding to positions 82−88 and 243−249 and 14 β-strands in the positions 48−54, 93−96, 99−104, 118−125, 129−133, 136−142, 152−156, 172−177, 184−189, 217−224, 229−234, 237−239, 258−264, and 284−297. This pattern is typical for family 16 β-endoglucanase (*3*).

Equilibrium Transition Studies in GdmCl at pH 2.0. At pH 2.0, incubation of endoglucanase in the presence of GdmCl induces structural changes, as indicated by the alterations of the far-UV CD and fluorescence spectra (Figure 2). The far-UV CD spectra analyzed at 220 nm upon increase of denaturant concentration show a decrease of the negative ellipticity above 4 M GdmCl with a small amplitude transition (Figure 6A). The changes in the far-UV CD spectra induced by GdmCl are reversible only above 4 M denaturant concentration, below this concentration the enzyme does not regain its native dichroic activity (Figure 6A). The global changes in the spectral 213−250-nm region were analyzed by SVD, which indicates that only two spectral components contribute to the far-UV CD spectra. The most significant singular values are 51.5, 8.4, and 2.8. All the other singular values are below 10% of the largest singular value and progressively decrease approaching to zero. A plot of the first and the second columns of the **V** matrix (V_1 and V_2) as a function of GdmCl concentration (data not shown) shows

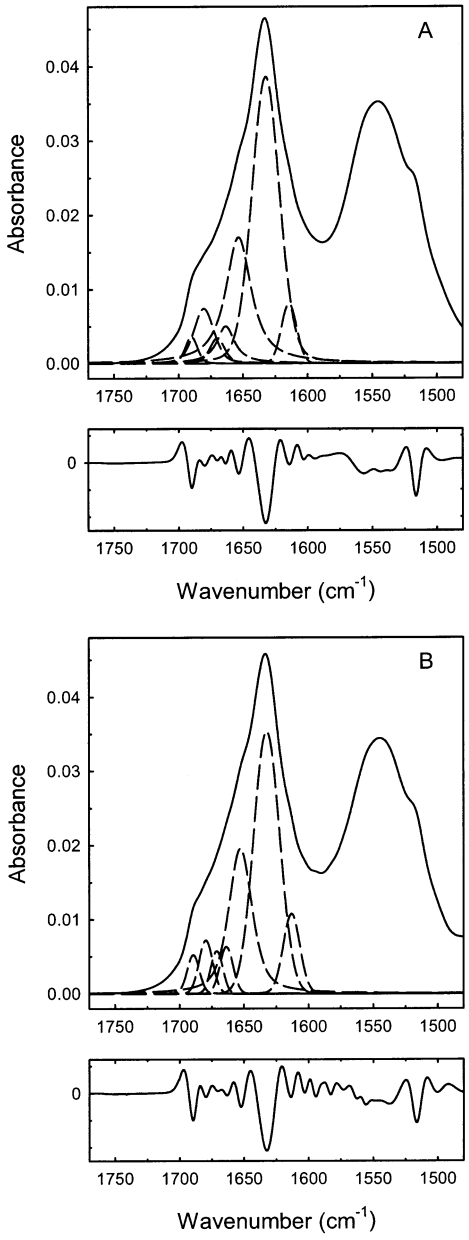

FIGURE 5: Effect of pH on the amide spectra of *P. furiosus* endoglucanase. Solution ATR-FTIR spectra of 8 mg/mL protein were measured in a CIRCLE cell with a Si crystal rod at 20 °C in 20 mM Tris-Cl at pH 7.4 (A) and at pH 2.0 (B). A total of 512 interferograms at 2 cm^{-1} resolution were collected for each spectrum. Deconvolution of the amide spectrum was used to identify the individual components in the amide I region by curve-fitting of the raw spectrum. The panels show the second derivative of the raw spectra.

transition profiles comparable to those observed by monitoring the 220-nm ellipticity changes.

The changes in the fluorescence spectra at denaturant concentration lower than 4 M are mainly due to the increase in fluorescence intensity (Figure 6B). Intrinsic fluorescence emission intensity progressively increases up to 3.5-fold between 0 and 4 M GdmCl concomitantly with a first red-shift of the maximum fluorescence emission wavelength from 335 to 345 nm (Figure 6C). Above 4 M denaturant, the maximum fluorescence emission wavelength abruptly shifts to 360 nm with a sigmoidal profile whereas the intrinsic fluorescence emission intensity, after a 30% decrease between 3.6 and 4.8 M GdmCl, increases up to 8.0 M denaturant (Figure 6B,C). The total amplitude of the intrinsic fluorescence emission intensity changes during the transition corresponds to a 4.5-fold increase. Similarly to far-UV CD spectral properties, reversibility was observed only above 4 M denaturant concentration (Figure 6B).

Table 2: Peak Position and Secondary Structure Assignment of the Amide I Bands of *P. furiosus* Endoglucanase

peak position (cm^{-1})	area (%) pH 7.4	area (%) pH 2.0 20 °C	area (%) pH 2.0 90 °C	assignment
1689	2.1	3.8	2.3	antiparallel β-sheets and aggregated strands
1680	7.9	5.7	24.7	turns
1670	2.9	4.2	0.0	turns
1664	6.1	5.3	1.8	turns
1653	28.0	30.1	38.3	α-helices and unordered structure
1632	53.0	50.9	32.9	β-sheets

Thermal Unfolding. The enzyme did not show any far-UV CD spectral change upon heating from 10 to 95 °C at pH 7.4 and pH 3.0 (data not shown). At pH 2.0, however, the thermal transition was characterized by remarkable changes of the far-UV CD spectral properties, in the absence of an isodichroic point (Figure 7). In particular, the progressive blue-shift of the zero intercept is accompanied by a decrease of the positive ellipticity at 194 nm and by a general increase of the negative ellipticity (Figure 7). At 90 °C the spectrum is characterized by a minimum at 205 nm and by the absence of positive ellipticity. The temperature-induced ellipticity changes at 208 and 198 nm, where the main amplitude was observed, occur in comparable non-two-state transitions, as shown in the inset of Figure 7. The native ellipticity could be restored up to about 60 °C during the cooling phase, below this temperature the thermal transition was irreversible (Figure 7, inset).

These results were paralleled by the data obtained following the temperature-induced changes on the FTIR spectra of the enzyme at pH 2.0 after deconvolution of the amide I region. At 90 °C, similarly to the spectrum deconvolution at 20 °C, six individual peaks were observed at 1689, 1680, 1664, 1653, 1632, and 1614 cm^{-1}, and only the peak centered at 1670 cm^{-1} was absent. The main peak at 1632 cm^{-1} was consistently reduced to 32.9% of the total area of the amide I region (Table 2) whereas the peak at 1653 cm^{-1}, which is in a spectral region where α-helices and unordered structure can equally contribute, was increased to 38.3%. The decrease in the amount of secondary structure elements at 90 °C was paralleled by an increased contribution of tyrosine ring vibrations at 1614 cm^{-1}. The peaks assigned to turns increased to 26.5% of the total amide I area at 90 °C, with the prevalence of the peak at 1680 cm^{-1} over the others (Table 2). Reversibility was observed up to about 60 °C during the cooling phase, similar to what was described for the ellipticity changes induced by temperature at pH 2.0.

DISCUSSION

The *P. furiosus* endoglucanase exhibits an outstanding stability against chemical and physical denaturation. The enzyme structure is in fact preserved under extreme conditions such as 95 °C at pH 3.0 and 7.9 M GdmCl. The tertiary structure perturbation induced by GdmCl and monitored by fluorescence changes is not accompanied by any measurable

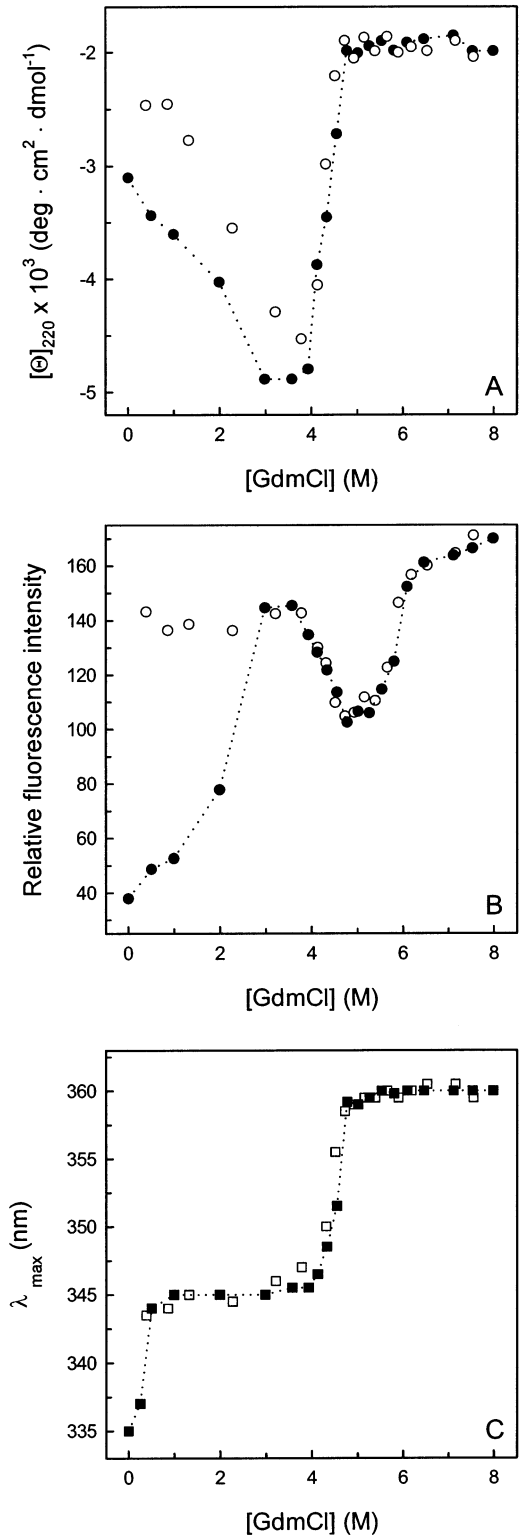

FIGURE 6: GdmCl-induced spectral changes of *P. furiosus* endoglucanase at pH 2.0. (A) Far-UV CD changes at 220 nm (●, ○) monitored in a 0.2-cm quartz cuvette. (B) Intrinsic relative intensity fluorescence (●, ○). (C) Maximum emission wavelength λ_{max} (■, □) changes. The dotted lines have the purpose to guide the eye of the reader and do not represent the fitting of the data. Reversibility points are indicated by empty symbols. All the spectra were recorded at 20 °C after 24-h incubation at the indicated GdmCl concentrations at 40 μg/mL protein concentration.

perturbation of the secondary structure elements. The discrepancy between the tertiary structure changes and the stability of the secondary structure elements is particularly

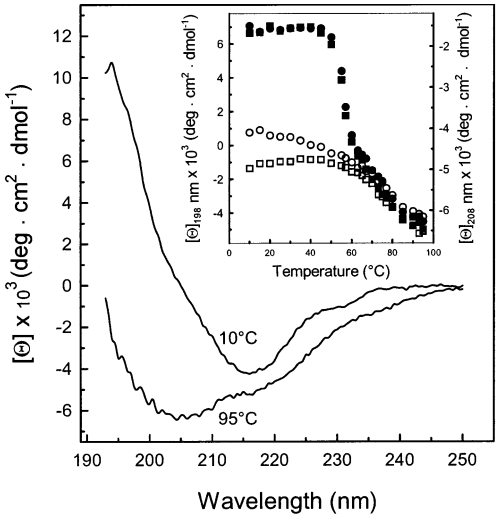

FIGURE 7: Thermal denaturation of *P. furiosus* endoglucanase at pH 2.0. The far-UV CD spectra were monitored at 5 °C interval during the heating cycle (10−95 °C). The spectra are reported after removal of the high-frequency noise and the low-frequency random error by SVD. The inset shows the molar ellipticity changes at 208 nm (●, ○) and at 198 nm (■, □) during the heating cycle. Empty symbols represent the molar ellipticity changes monitored during the cooling cycle.

interesting because the far-UV CD signal during the titrations with the denaturant is unchanged up to 8 M GdmCl. The analysis of the near-UV CD spectrum of the protein in 7.9 M GdmCl indicates that the tertiary structure arrangement is altered but not suppressed because the disappearance of the 295-nm band of Trp is not paralleled by the loss of the asymmetric environment for all the aromatic residues that still contribute to the fine structure of the spectrum. The suppression of the 295 nm band and the concomitant red-shift of the intrinsic fluorescence maximum emission wavelength indicate that the change in the asymmetric environment for Trp residues is accompanied, at least in part, by solvent exposure. The reversible sigmoidal transition of the fluorescence changes upon denaturant addition suggests a two-state process, which leads to the formation of a 7.9 M GmCl state with the same secondary structure elements of the native state and with a different tertiary arrangement. The presence of residual structural elements at high concentration of GdmCl has been reported for different proteins (*8*, *38*, *39*). *P. furiosus* endoglucanase is, to the best of our knowledge, the first protein that retains residual tertiary contacts still locked in 7.9 M GdmCl.

Interestingly, the proteins containing residual structural elements at high GdmCl concentrations are mostly characterized by β-structure, which may form hydrophobic clusters in antiparallel β-sheet at high denaturant concentration (*8*, *9*, *40*). The *P. furiosus* endoglucanase has indeed a high content of β structure, as indicated by the comparable estimation of its secondary structure elements by deconvolution of far-UV CD and FTIR spectra, which both indicate the prevalence of β elements (about 50%) over other secondary structure elements. A high content of β structure, as determined by far-UV CD spectroscopy, characterizes also the thermophilic family 16 endoglucanase from *Rhodothermus marinus* (*7*). This is a common feature of family 16 glycosyl hydrolases (*2*) to which *P. furiosus* endoglucanase has been assigned on the basis of its primary structure (*1*).

The presence of antiparallel β-sheets and turns revealed by deconvolution of the amide I region suggests also for *P. furiosus* endoglucanase a compact jellyroll-type β-sheet structure according to the 3D structure analysis of family 16 glycosyl hydrolases (*2*). These proteins share a similar fold usually characterized by 12−14 antiparallel β-strands arranged in two sheets that pack against each other (*6*). The identification in *P. furiosus* endoglucanase, by secondary structure prediction (*37*), of 14 β-strands is in line with the assignment of this protein to the family 16 glycosyl hydrolases. These proteins fold into a compact jellyroll-type β-sheet structure like the concanavalin A-like lectins, a family of carbohydrate binding proteins with high values of conformational stability mainly related to intersubunit interactions (*41*, *42*). Notably, in *P. furiosus* endoglucanase the β-strands corresponding to residues 217−224, 258−264, and 284−297 are mainly composed of aromatic and hydrophobic amino acid residues with a very low relative solvent accessibility (*37*). These hydrophobic clusters may be involved in hydrophobic interactions possibly responsible for the presence of residual structure in 7.9 M GdmCl, similar to what was reported for other proteins (*8*, *40*).

The thermodynamic parameters derived from the fluorescence changes upon increasing GdmCl are suggestive of the high intrinsic stability of the archaeal endoglucanase with a ΔG^{H_2O} of 15.4 kcal/mol, a value at the upper limit of the stability for a globular protein, and a transition midpoint at 6.7 M GdmCl. The presence of a significant residual structure at 7.9 M GdmCl clearly indicates that the ΔG measurement may not reflect the free energy difference between the unique native state and the denatured states. Hence the value of 15.4 kcal/mol is almost surely a lower limit on the stability of *P. furiosus* endoglucanase. The analysis of the effect of pH on the protein spectral properties showed that the secondary structure elements are preserved down to pH 1.0 whereas only the protein at pH 2.0 shows a near-UV CD spectrum closely similar to that at pH 7.4. This result indicates that at pH 2.0 the increased exposure of the hydrophobic residues may not significantly affect the tertiary structure arrangement and led us to study the combined effect of low pH and denaturant on the protein structural stability. The analysis of the spectral changes induced by GdmCl at pH 2.0 indicates a complex process. The identification, by SVD analysis of the far-UV CD data, of two spectral components that both respond in a concerted manner to GdmCl-induced changes suggests that the differences observed among the transition profiles monitored by ellipticity, intrinsic fluorescence intensity, and maximum emission wavelength are not related to the presence of distinct partially folded forms with different secondary structure arrangements. The increase in negative ellipticity observed between 0.5 and 3 M GdmCl may be ascribed to the different contribution of the 11 Trp residues to the far-UV CD spectrum (*43*), which would be in agreement with the concomitant changes in intrinsic fluorescence intensity. The changes in secondary structure, indeed, occur between 3.0 and 5.0 M GdmCl and are paralleled by the exposure of Trp residues as indicated by the red-shift of the fluorescence maximum emission wavelength.

The relevant stability of *P. furiosus* endoglucanase is also shown by the lack of effect of temperature on the secondary structure elements, which are all preserved up to 90 °C at pH 7.4 and pH 3.0. The far-UV CD spectral changes observed during the thermal transition at pH 2.0 are characterized by a general increase of the negative ellipticity and may be tentatively ascribed to different contribution of aromatic residues to the far-UV CD spectrum (*43*), to an increase in turns (*44*), and/or to unordered structure (*45*). A comparative analysis of the FTIR spectral changes observed at 90 °C at pH 2.0 indicates that the secondary structure is altered, mainly because of the relative increase of β turns accompanied by a decrease of β-sheets. The changes in the relative contributions of the different secondary structure elements clearly show that the secondary structure is reduced but not abolished and suggest that the protein at 90 °C and pH 2.0 is in a "partially denatured" state.

The residual structure present after thermal unfolding is in line with the results obtained in the presence of GdmCl and points to a significant structural stability of this protein. The structured denatured states, observed in β-proteins rich in hydrophobic clusters, have been related with the hypothesis that they may serve as "seeds" to initiate the folding process (*8*, *40*). The specific regions of *P. furiosus* endoglucanase primary sequence rich in hydrophobic amino acid residues with a very low solvent accessibility may form hydrophobic clusters responsible of the persistence of residual tertiary structure under extremely denaturing conditions. The selection of specific sites for mutagenesis to identify the role played by individual residues in the formation of highly resistant β strands should be supported by the resolution of the crystal structure. A relevant number of primary sequences of family 16 enzymes is available; however, the crystal structure is known only for a few mesophilic glycosyl hydrolases (*46*) from this family, and three-dimensional data from hyperthermophilic sources are not available.

REFERENCES

1. Gueguen, Y., Voorhorst, W. G., van der Oost, J., and de Vos, W. M. (1997) Molecular and biochemical characterization of an endo-β-1,3-glucanase of the hyperthermophilic archaeon *Pyrococcus furiosus*, *J. Biol. Chem. 272*, 31258−31264.
2. Henrissat, B., and Coutinho, P. M. (2001) Classification of glycoside hydrolases and glycosyltransferases from hyperthermophiles, *Methods Enzymol. 330*, 183−201.
3. Planas, A. (2000) Bacterial 1,3-1,4-β-glucanases: structure, function and protein engineering, *Biochim. Biophys. Acta 1543*, 361−382.
4. Murzin, A. G., Brenner, S. E., Hubbard, T., and Chothia, C. (1995) SCOP: a structural classification of proteins database for the investigation of sequences and structures, *J. Mol. Biol. 247*, 536−540.
5. Krah, M., Misselwitz, R., Politz, O., Thomsen, K. K., Welfle, H., and Borriss, R. (1998) The laminarinase from thermophilic eubacterium *Rhodothermus marinus*. Conformation, stability, and identification of active site carboxylic residues by site-directed mutagenesis, *Eur. J. Biochem. 257*, 101−111.
6. Otzen, D. E., Christiansen, L., and Schulein, M. (1999) A comparative study of the unfolding of the endoglucanase Cel45 from *Humicola insolens* in denaturant and surfactant, *Protein Sci. 8*, 1878−1887.
7. Peumans, W. J., Barre, A., Derycke, V., Rouge, P., Zhang, W., May, G. D., Delcour, J. A., Van Leuven, F., and Van Damme, E. J. (2000) Purification, characterization and structural analysis of an abundant β-1,3-glucanase from banana fruit, *Eur. J. Biochem. 267*, 1188−1195.
8. Koepf, E. K., Petrassi, H. M., Sudol, M., and Kelly, J. W. (1999) WW: An isolated three-stranded antiparallel β-sheet domain that unfolds and refolds reversibly; evidence for a structured hydrophobic cluster in urea and GdnHCl and a disordered thermal unfolded state, *Protein Sci. 8*, 841−853.

9. Klein-Seetharaman, J., Oikawa, M., Grimshaw, S. B., Wirmer, J., Duchardt, E., Ueda, T., Imoto, T., Smith, L. J., Dobson, C. M., and Schwalbe, H. (2002) Long-range interactions within a nonnative protein, *Science 295*, 1719−22.
10. Radford, S. E. (2000) Protein folding: progress made and promises ahead, *Trends Biochem. Sci. 25*, 611−618.
11. Yutani, K., Takayama, G., Goda, S., Yamagata, Y., Maki, S., Namba, K., Tsunasawa, S., and Ogasahara, K. (2000) The process of amyloid-like fibril formation by methionine aminopeptidase from a hyperthermophile, *Pyrococcus furiosus*, *Biochemistry 39*, 2769−2777.
12. Gill, S. C., and von Hippel, P. H. (1989) Calculation of protein extinction coefficients from amino acid sequence data, *Anal. Biochem. 182*, 319−326.
13. Oberg, K. A., and Fink, A. L. (1998) A new attenuated total reflectance Fourier transform infrared spectroscopy method for the study of proteins in solution, *Anal. Biochem. 256*, 92−106.
14. Anderson, S., and Weber, G. (1966) The reversible acid dissociation and hybridization of lactic dehydrogenase, *Arch. Biochem. Biophys. 116*, 207−223.
15. Royer, C. A., Mann, C. J., and Matthews, C. R. (1993) Resolution of the fluorescence equilibrium unfolding profile of trp aporepressor using single tryptophan mutants, *Protein Sci. 2*, 1844−1852.
16. Henry, E. R., and Hofrichter, J. (1992) Singular value decomposition: application to analysis of experimental data, *Methods Enzymol. 210*, 129−192.
17. Johnson, W. C., Jr. (1992) Analysis of circular dichroism spectra, *Methods Enzymol. 210*, 426−447.
18. Ionescu, R. M., Smith, V. F., O'Neill, J. C., Jr., and Matthews, C. R. (2000) Multistate equilibrium unfolding of *Escherichia coli* dihydrofolate reductase: thermodynamic and spectroscopic description of the native, intermediate, and unfolded ensembles, *Biochemistry 39*, 9540−9550.
19. Clark, A. H., Saunderson, D. H., and Suggett, A. (1981) Infrared and laser-Raman spectroscopic studies of thermally induced globular protein gels, *Int. J. Pept. Protein Res. 17*, 353−364.
20. Susi, H., and Byler, D. M. (1983) Protein structure by Fourier transform infrared spectroscopy: second derivative spectra, *Biochem. Biophys. Res. Commun. 115*, 391−397.
21. Casal, H. L., Kohler, U., and Mantsch, H. H. (1988) Structural and conformational changes of β-lactoglobulin B: an infrared spectroscopic study of the effect of pH and temperature, *Biochim. Biophys. Acta 957*, 11−20.
22. Arrondo, J. L. R., Muga, A., Castresana, J., Bernabeu, C., and Goñi, F. M. (1989) An infrared spectroscopic study of β-galactosidase structure in aqueous solution, *FEBS Lett. 252*, 118−120.
23. Arrondo, J. L., Castresana, J., Valpuesta, J. M., and Goni, F. M. (1994) Structure and thermal denaturation of crystalline and noncrystalline cytochrome oxidase as studied by infrared spectroscopy, *Biochemistry 33*, 11650−11655.
24. Jackson, M., and Mantsch H. H. (1995) The use and misuse of FTIR spectroscopy in the determination of protein structure, *Crit. Rev. Biochem. Mol. Biol. 30*, 95−120.
25. Xie, L., Jing, G. Z., and Zhou, J. M. (1996) Reversible thermal denaturation of staphylococcal nuclease: a Fourier transformed infrared spectrum study, *Arch. Biochem. Biophys. 328*, 122−128.
26. Dong, A., Kery, V., Matsuura, J., Manning, M. C., Kraus, J. P., and Carpenter, J. F. (1997) Secondary structure of recombinant human cystathionine beta-synthase in aqueous solution: effect of ligand binding and proteolytic truncation, *Arch. Biochem. Biophys. 344*, 125−132.
27. Fabian, H., Falber, K., Gast, K., Reinstadler, D., Rogov, V. V., Naumann, D., Zamyatkin, D. F., and Filimonov, V. V. (1999) Secondary structure and oligomerization behavior of equilibrium unfolding intermediates of the λ Cro repressor, *Biochemistry 38*, 5633−5642.
28. Garcia-Garcia, J., Gomez-Fernandez, J. C., and Corbalan-Garcia, S. (2001) Structural characterization of the C2 domain of novel protein kinase Cϵ, *Eur. J. Biochem. 268*, 1107−1117.
29. Santoro, M. M., and Bolen, D. W. (1988) Unfolding free energy changes determined by the linear extrapolation method. 1. Unfolding of phenylmethanesulfonyl alpha-chymotrypsin using different denaturants, *Biochemistry 27*, 8063−8068.
30. Pace, C. N. (1990) Conformational stability of globular proteins, *Trends Biochem. Sci. 15*, 14−17.
31. Woody, R. W. (1995) Circular dichroism, *Methods Enzymol. 246*, 34−71.
32. Tilstra, L., and Mattice, W. L. (1996) The β sheet D coil transition of polypeptides, as determined by circular dichroism, in *Circular Dichroism and the Conformational Analysis of Biomolecules* (Fasman, G. D., Ed.) pp 261−283, Plenum Press, New York.
33. Deléage, G., and Geourjon, C. (1993) Dicroprot: An interactive graphic program for calculating the secondary structures content of proteins from circular dichroism spectrum, *Comput. Appl. Biosci. 9*, 197−199.
34. Greenfield, N. J. (1996) Methods to estimate the conformation of proteins and polypeptides from circular dichroism data, *Anal. Biochem. 235*, 1−10.
35. Malin, E. L., Alaimo, M. H., Brown, E. M., Aramini, J. M., Germann, M. W., Farrell, H. M., Jr., McSweeney, P. L., and Fox, P. F. (2001) Solution structures of casein peptides: NMR, FTIR, CD, and molecular modeling studies of alphas1-casein, 1−23, *J. Protein Chem. 20*, 391−404.
36. Barth, A. (2000) The infrared absorption of amino acid side chains, *Prog. Biophys. Mol. Biol. 74*, 141−73.
37. Rost, B. (1996) PHD: predicting one-dimensional protein structure by profile-based neural networks, *Methods Enzymol. 266*, 525−539.
38. Kuwajima, K., Yamaya, H., and Sugai, S. (1996) The burst-phase intermediate in the refolding of β-lactoglobulin studied by stopped-flow circular dichroism and absorption spectroscopy, *J. Mol. Biol. 264*, 806−822.
39. Shortle, D., and Ackerman, M. S. (2001) Persistence of native-like topology in a denatured protein in 8 M urea, *Science 293*, 487−489.
40. Martensson, L. G., Jonsson, B. H., Freskgard, P. O., Kihlgren, A., Svensson, M., and Carlsson, U. (1993) Characterization of folding intermediates of human carbonic anhydrase II: probing substructure by chemical labeling of SH groups introduced by site-directed mutagenesis, *Biochemistry 32*, 224−231.
41. Loris, R. (2002) Principles of structures of animal and plant lectins, *Biochim. Biophys. Acta 1572*, 198−208.
42. Mitra, N., Srinivas, V. R., Ramya, T. N., Ahmad, N., Reddy, G. B., and Surolia, A. (2002) Conformational stability of legume lectins reflect their different modes of quaternary association: solvent denaturation studies on concanavalin A and winged bean acidic agglutinin, *Biochemistry 41*, 9256−9263.
43. Woody, R. W. (1996) Aromatic and cystine side-chain circular dichroism proteins, in *Circular Dichroism and the Conformational Analysis of Biomolecules* (Fasman, G. D., Ed.) pp 109−157, Plenum Press, New York.
44. Perczel, A., and Hollosi, M. (1996) Turns, in *Circular Dichroism and the Conformational Analysis of Biomolecules* (Fasman, G. D., Ed.) pp 285−380, Plenum Press, New York.
45. Privalov, P. L., Tiktopulo, E. I., Venyaminov, S. Yu., Griko, Yu. V., Makhatadze, G. I., and Khechinashvili, N. N. (1989) Heat capacity and conformation of proteins in the denatured state, *J. Mol. Biol. 205*, 737−750.
46. Coutinho, P. M., and Henrissat, B. (1999) Carbohydrate-Active Enzymes (http://afmb.cnrs-mrs.fr/~pedro/CAZY/db.html).

BI026498U